Bridging the PE Lifetime under Fatigue and Creep Conditions with Its Crystallization Behavior

K. KADOTA,[1] S. CHUM,[2] and A. CHUDNOVSKY[1,*]

[1]Department of Civil Engineering, Mechanics and Metallurgy (M/C246) University of Illinois at Chicago, P.O. Box 4348, Chicago, Illinois 60680; [2]The Dow Chemical Company, Polyethylene Division, Highway 227, Freeport, Texas 77541

SYNOPSIS

The service lifetime for several linear polyethylene copolymers was studied by fatigue-type accelerated tests. The material morphology and crystallization behavior were correlated with the lifetime and the failure modes. The correlation is based on the rate constant of material degradation (RCMD) recently introduced by the authors within a mathematical model for crack layer growth kinetics. RCMD is found to depend on the loading conditions (e.g., creep or fatigue) and on material morphology reflected in crystallization kinetics. The ratio of RCMDs for fatigue and creep is a scaling factor that allows one to correlate fatigue and creep lifetimes. The dependence of the RCMD's ratio on the morphological features associated with the primary and secondary crystallization kinetics is also reported in this paper. © 1993 John Wiley & Sons, Inc.

INTRODUCTION

Polyethylene (PE) is widely used in gas and water distribution pipes. The piping system in such applications is expected to function properly up to 20–50 years and more. Thus, there is a pressing quest for an accelerated test procedure to predict the long-term service life. For this purpose, a fatigue-type loading is widely used as an accelerating factor.[1–9] It seems plausible since (a) PE fracture under fatigue and creep conditions exhibits many common features and (b) fatigue conditions in most cases significantly reduce the time to failure in comparison with creep.[5–7] In general, lifetime under creep and fatigue correlates well for various PEs. However, some exceptions from the general trend reported by Zhou et al.[1] indicate a limitation of an empirical approach and call for further understanding and modeling of PE fracture.

A thorough study of crack initiation and growth under fatigue and creep conditions in PEs with various branch densities were reported by Zhou et al.[1] It was observed that the lifetime under creep monotonically increases with branch density, whereas the fatigue lifetime exhibits a nonmonotonic dependency, especially in the low branch density range.

In this paper, the difference in the material morphology of the specimens tested by Zhou, et al.[1] is examined from the crystallization kinetics point of view. A mathematical model of the crack growth[10] is employed to analyze the creep and fatigue crack growth mechanisms. A correlation of creep and fatigue lifetime in terms of two morphological parameters associated with the primary and secondary crystallization is reported.

FRACTOGRAPHIC STUDY

To use the fatigue test as an accelerated test for the creep, a similarity in fracture mechanisms has to be established. Figures 1 and 2 are SEM micrographs of the fracture surfaces of two different PEs formed under fatigue and creep. The details of the test conditions are described in Ref. 1. Striations, which are evidence of discontinuous crack growth, can be clearly observed on the fatigue fracture surfaces. Although one can also see a few lines on the creep

* To whom correspondence should be addressed.

Journal of Applied Polymer Science, Vol. 49, 863–875 (1993)
 CCC 0021-8995/93/050863-13

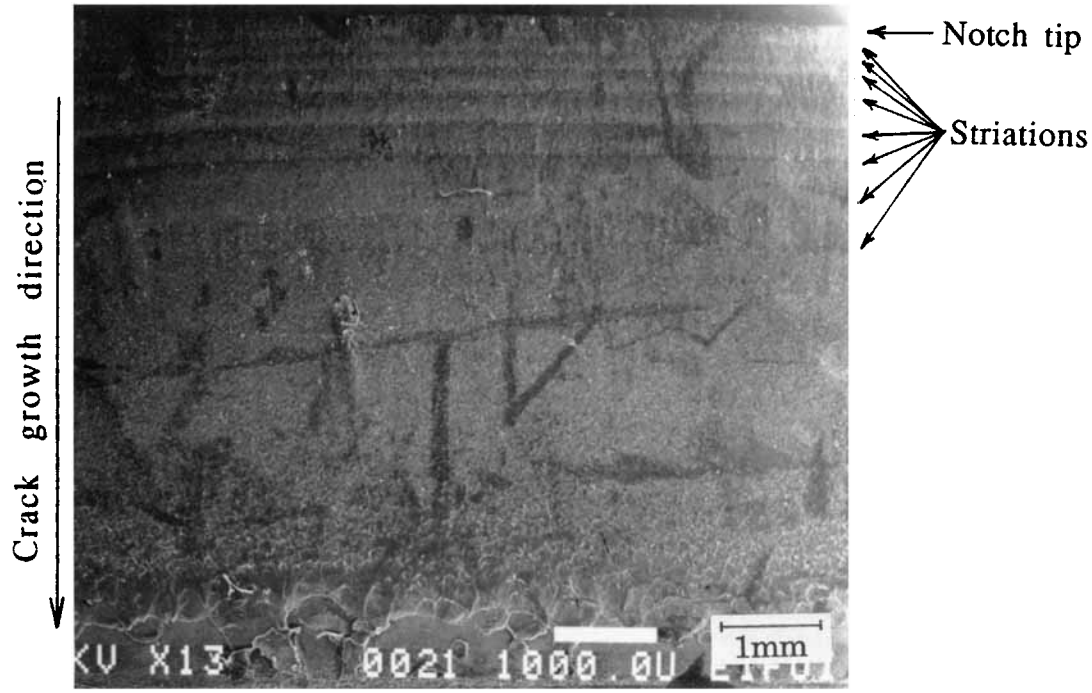

(a) M5202 resin (Branch Density=1.2).

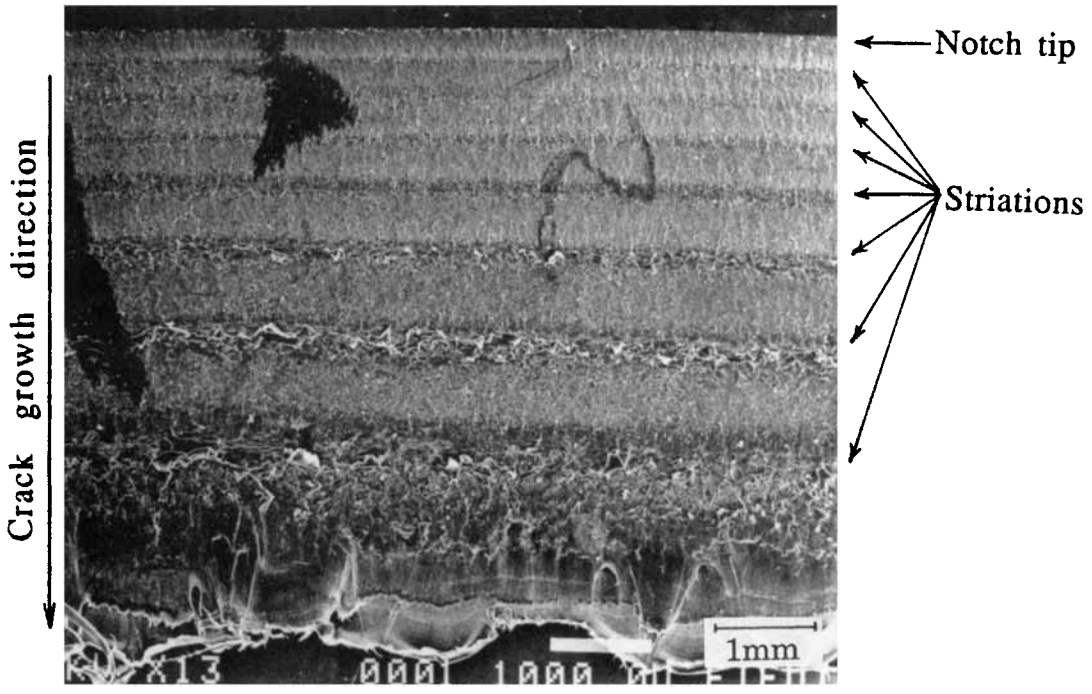

(b) TR140 resin (Branch Density=2.3).

Figure 1 SEM micrograph of the fatigue fracture surfaces: (a) M5202 resin (branch density = 1.2); (b) TR140 resin (branch density = 2.3).

(a) M5202 resin (Branch Density=1.2).

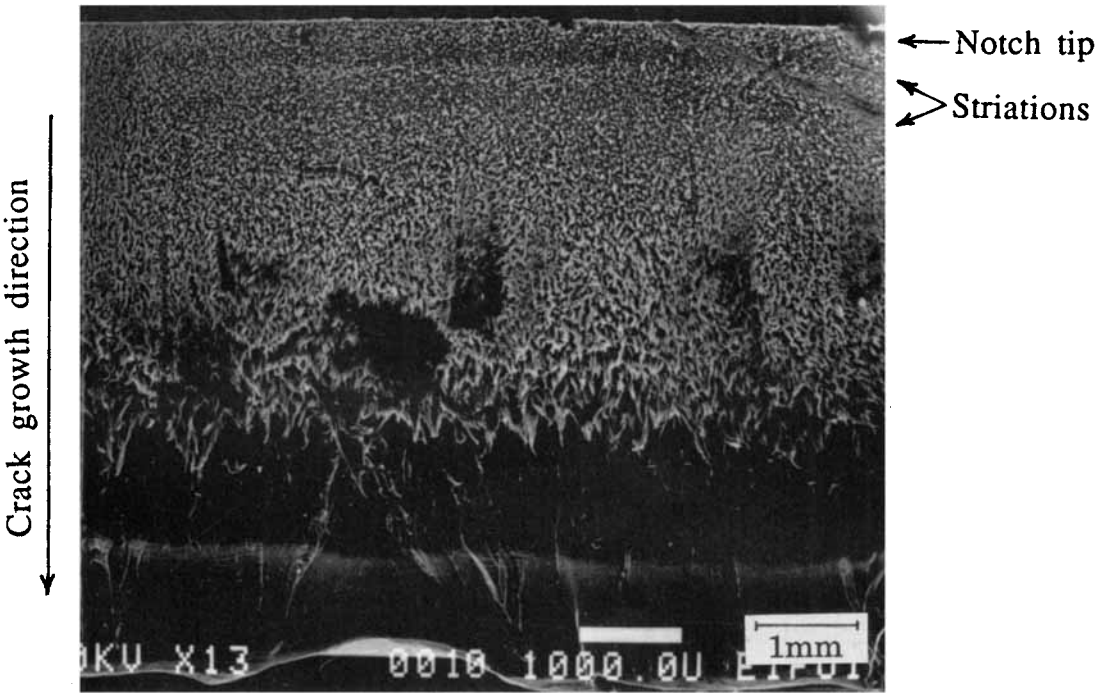

(b) TR140 resin (Branch Density=2.3).

Figure 2 SEM micrograph of the creep fracture surfaces: (a) M5202 resin (branch density = 1.2); (b) TR140 resin (branch density = 2.3).

fracture surface of TR140 resin, for instance (Fig. 2), the striations are not as visible on the creep fracture surfaces. Nevertheless the discontinuous crack growth is well documented for both creep and fatigue-loading conditions at relatively low stress.[1-8,11] Lu et al. reported that the arrest lines are not always visible at a low stress level since the intrinsic size of the fibrils tends to obscure the arrest lines when they are very finely spaced.[11] The applied stress of the creep experiment in Ref. 1 is in the range 10–15% of the yielding stress σ_y, suggesting a discontinuous crack growth mode under creep as well as fatigue.

Figures 3 and 4 are SEM micrographs of the fracture surfaces (same as Fig. 1 and 2) at a higher magnification. Apparently, the fatigue and creep fracture surfaces have different appearances. As for the fatigue fracture surface under tension–tension cyclic loading, the evolution of microfeatures (cellular pattern) on the fracture surface has been observed (Fig. 5).[12] The size of cellular features was directly related to the crack driving force (energy release rate), i.e., the average radius of the cells is proportional to the energy release rate.[12] For the tension–compression ($\sigma_\infty = \pm 4$ MPa) loading cycles employed in the testing program reported in Ref. 1, such a pattern is difficult to observe in Figure 4. However, using a higher magnification, one can see similar features formed under tension–compression cycles (Fig. 6).

The creep fracture surfaces have a more fibrous nature; still, we observed creep similar to the fatigue

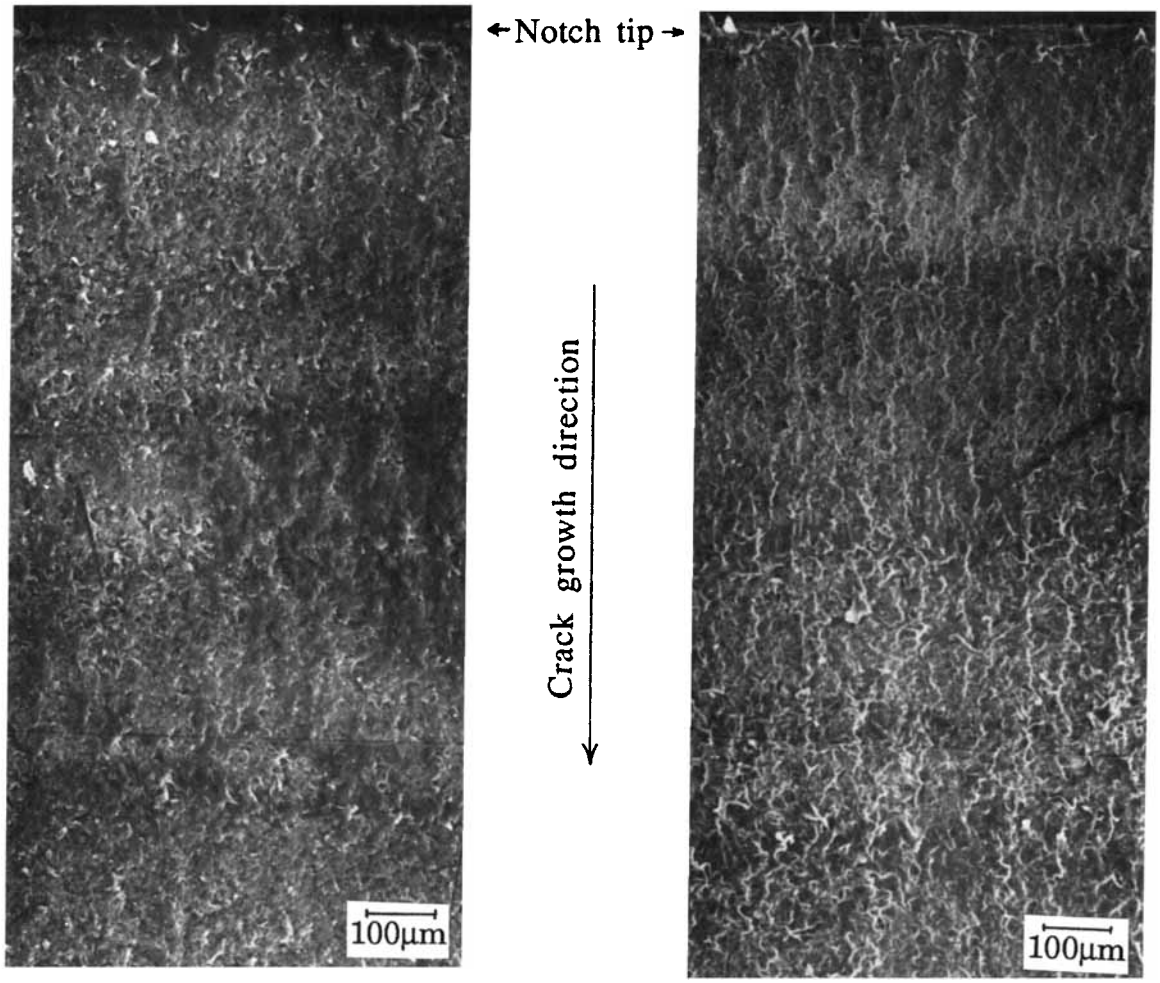

Figure 3 SEM micrograph of the fatigue fracture surfaces (same as Fig. 1): (a) M5202 resin (branch density = 1.2); (b) TR140 resin (branch density = 2.3).

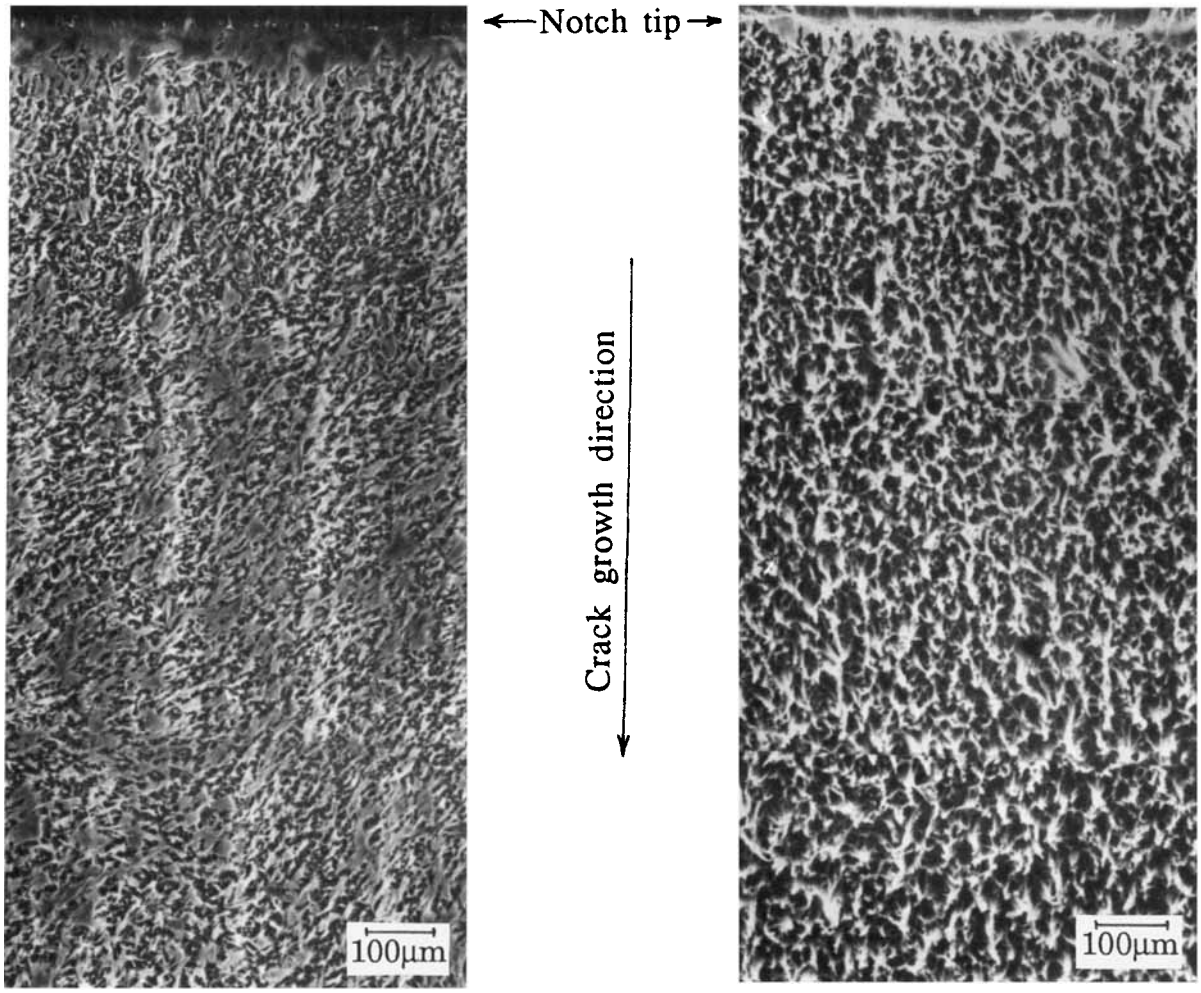

Figure 4 SEM micrograph of the creep fracture surfaces (same as Fig. 2): (a) M5202 resin (branch density = 1.2); (b) TR140 resin (branch density = 2.3).

trends. A distance between adjacent fibers is measured as a characteristic size instead of the radius of cellus. Figure 7 shows the relation between this characteristic size and the energy release rate. The average size is proportional to the energy release rate. Although the microfeatures of the fracture surfaces are different, the creep fracture surface shows the same trend as that of the fatigue fracture surface. Based on that, the formation of the process zone under creep and fatigue can be treated as similar. To establish a quantitative similarity criterion in the fracture mechanism, a further systematic analysis of the fracture surfaces is required (e.g., the relation between creep and fatigue in terms of proportionality coefficients of the characteristic size on the fracture surface vs. the energy release rate).

CRACK GROWTH ANALYSIS

Assuming that the similarity between creep and fatigue exists, the point in question is the discrepancy in the relation between creep and fatigue lifetimes. The results from Zhou et al.[1] are addressed here. The lifetime itself depends on many factors, e.g., type of loading, applied stress level, and temperature. Especially, the maximum applied stress of the fatigue test (σ_{max} = 4 MPa) and the creep test (σ_{max} = 3 MPa) are different in Ref. 1. Thus, we would like to pick up a certain parameter that reflects the type of loading (i.e., constant load vs. cyclic load), but does not depend on a particular stress level. For this purpose, we employed the mathematical model

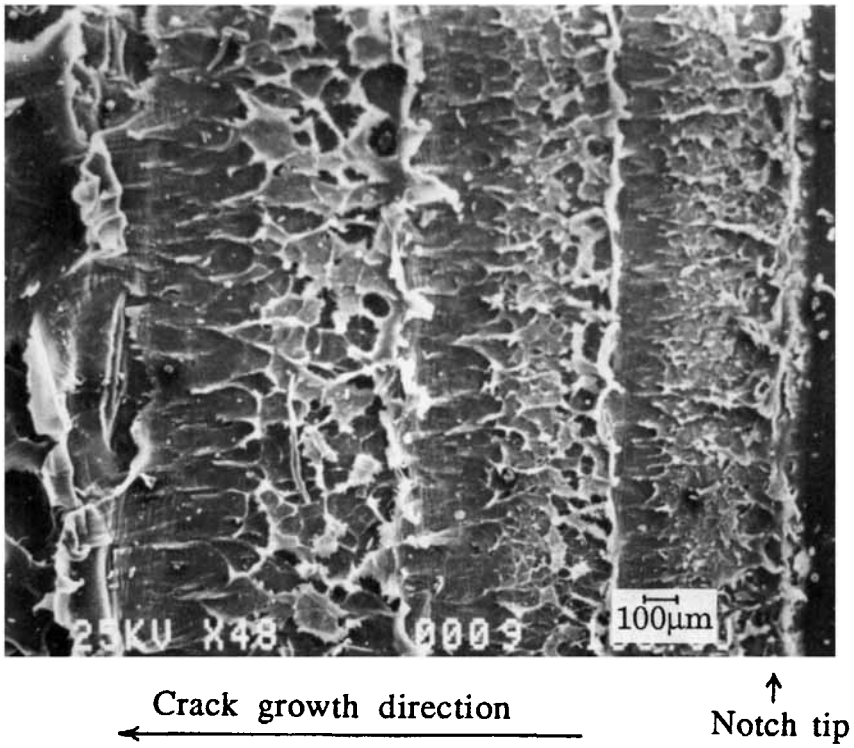

Figure 5 SEM micrograph of the tension–tension fatigue fracture surface.[11,12]

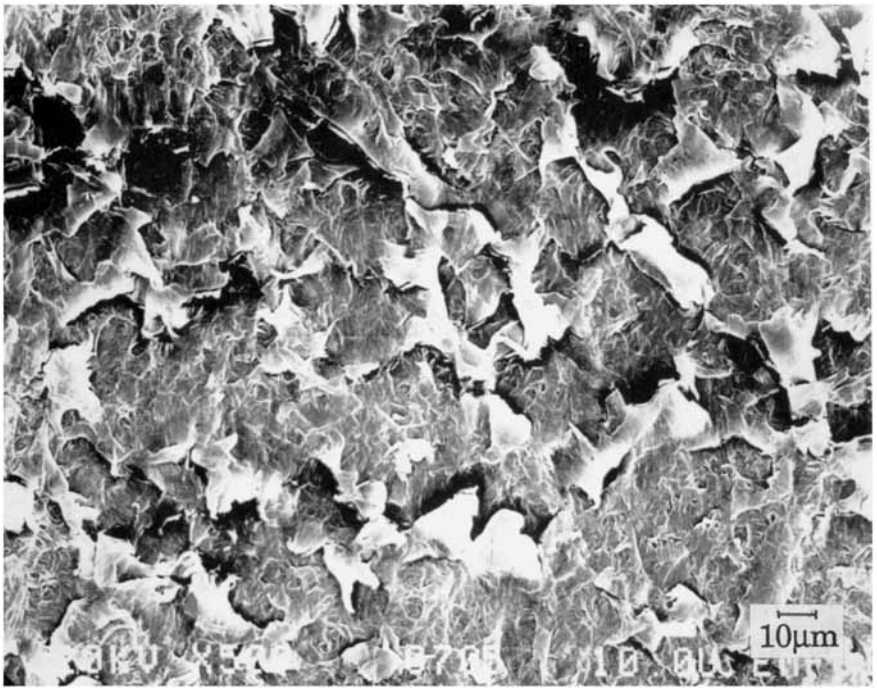

Figure 6 SEM micrograph of the tension–compression fatigue fracture surface of M5202 resin [same as Fig. 1(a)].

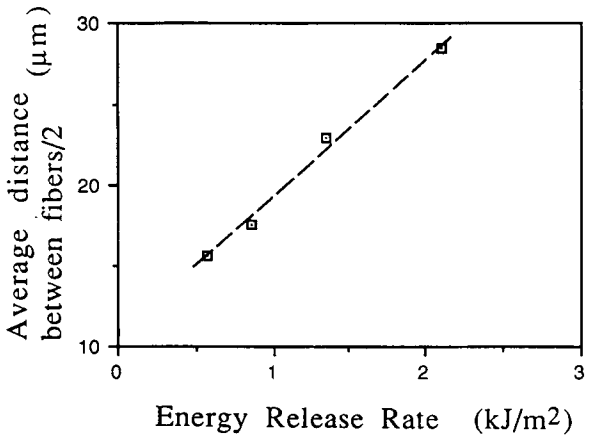

Figure 7 Average distance between fibers on the creep fracture surface vs. energy release rate (TR140 resin).

of crack growth in ductile polymer that was recently proposed by the authors.[10]

(a) Description of the Model

The process zone is modeled as a phase transformation localized in a thin strip ahead of the crack. Experimental observations supporting this consideration are presented elsewhere.[11,13] We consider the crack and the process zone to be a single entity called the crack layer (CL). Figure 8 shows a schematic representation of the model: V_{tr}, is the domain occupied by the second phase (process zone); σ_∞, the applied stress; and l and l_a, the crack and process zone lengths, respectively. The material within the strip of width $w_0(x_1)$ undergoes transformation (drawing) at a constant draw ratio λ. The resulting process zone of width $w^*(x_1)$ is indicated by the solid line.

For computational purposes, the two-phase system is treated as the superposition of the two problems illustrated in Figure 9. One problem is obtained by removing the process zone and substituting an equivalent traction σ_{tr}. The constancy of σ_{tr} along the phase boundary follows from the phase equilibrium condition. The other problem is the process zone V_{tr} subjected to σ_{tr}, which represents the action of the original phase.

Using the assumption of a thin strip, V_{tr} is uniquely determined by the process zone length l_a for the given values of l and σ_∞. In this case, the Gibbs potential of the system (per unit thickness) can be expressed as a simple superposition of the potential energy Π of the first phase, the fracture energy $2\gamma l$ associated with crack propagation within the drawn material, and the product of the volume V_{tr} of the zone of transformed material and the jump γ_{tr} of the Gibbs potential density (per unit volume) across the boundary between the drawn and original material. The resulting equation is

$$G = \Pi + 2\gamma l + \gamma_{tr} V_{tr} + G_0 \tag{1}$$

where γ is the Griffith's fracture energy of the drawn material per unit area, and G_0, the reference level of the Gibbs potential.

Using basic thermodynamics, the driving forces for the crack, X^{CR}, and the process zone, X^{PZ}, can be expressed as partial derivatives of the Gibbs potential with respect to corresponding variables (the crack length l and the process zone size l_a):

$$X^{CR} = -\left.\frac{\partial G}{\partial l}\right|_{l+l_a=\text{const.}} \tag{2}$$

$$X^{PZ} = -\left.\frac{\partial G}{\partial l_a}\right|_{l=\text{const.}} \tag{3}$$

Employing a standard fracture mechanics formalism, the driving forces per unit thickness are[10,14,15]

$$\text{Crack driving force: } X^{CR} = J_1 - 2\gamma \tag{4}$$

Process zone driving force:

$$X^{PZ} = \frac{K^{tot}}{E_0}\left\{K^{tot} + \frac{2\gamma_{tr}}{\sigma_{tr}(\lambda - 1)} K[\sigma_{tr}]\right\} \tag{5}$$

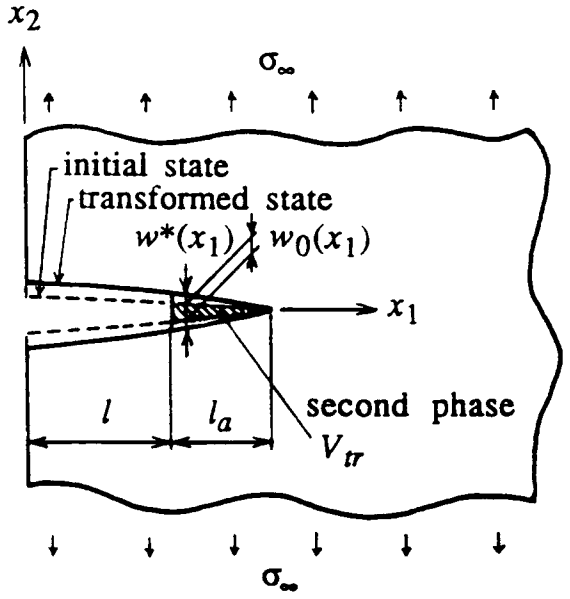

Figure 8 Model of the process zone as a phase transformation.

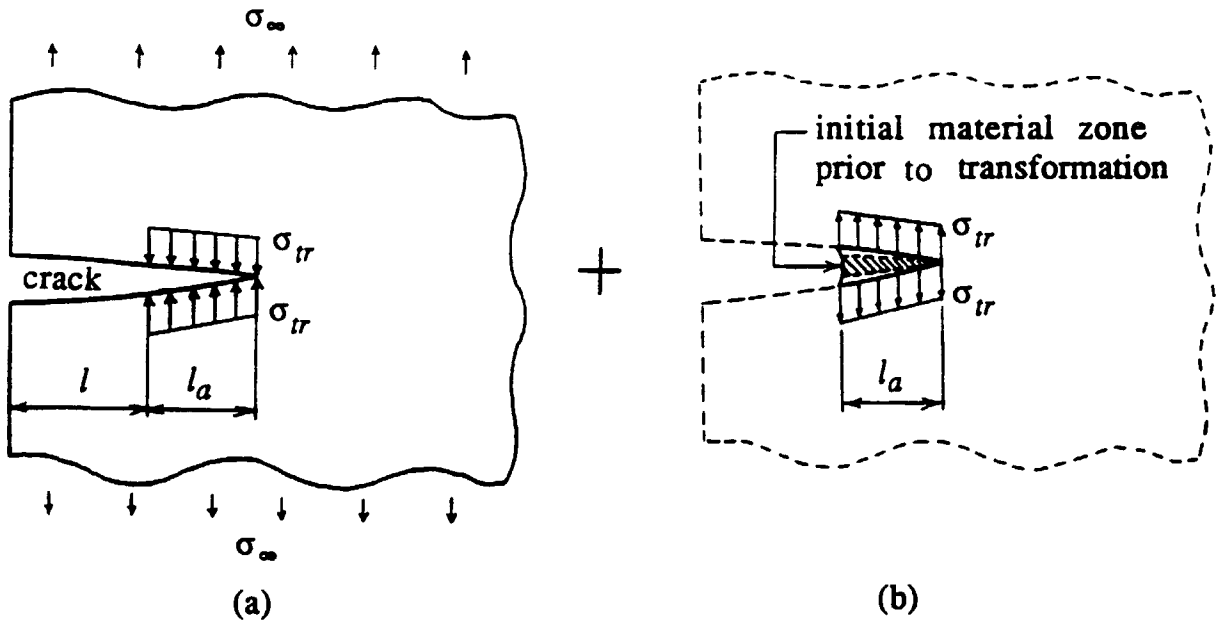

Figure 9 Decomposition of the problem depicted in Figure 8.

Here, the active part of the crack driving force (the energy release rate because of crack extension into a stationary process zone) is

$$J_1 = \sigma_{tr}\left\{\delta^{tot} + \frac{\gamma_{tr}}{\sigma_{tr}(\lambda - 1)}\,\delta[\sigma_{tr}]\right\} \tag{6}$$

K^{tot} is the stress intensity factor (SIF), and δ^{tot}, the crack tip opening displacement (CTOD at $x_1 = l$) for the problem shown in Figure 9 (a). $K[\sigma_{tr}]$ and $\delta[\sigma_{tr}]$ are, respectively, the SIF and CTOD for the same problem when $\sigma_\infty = 0$. E_0 is the Young's modulus of the initial material.

It is shown in Ref. 10 that the degradation of the material within the process zone by the action of the transformation stress σ_{tr} (reflected in the decrease of γ) is responsible for crack advance since the crack propagation does not occur if the crack resistance 2γ is greater than J_1. We consider that the material degradation resulting in the decay of fracture energy γ is a first-order reaction. Assuming that $\gamma = 0$ when the degradation is completed, γ can be expressed as

$$\gamma = \gamma_0 \exp(-k\{t - t_i(x_1)\}) \tag{7}$$

Here, γ_0 is the initial value of the fracture energy at time $t_i(x_1)$ of material transformation at the point x_1, and k, a rate constant that obeys an Arrhenius-type equation.[16]

The kinetic equations for the crack layer growth are proposed in the simplest form of Onsager-type linear relations between the rates of the crack and process zone growth and conjugate forces:

$$\dot{l} = k_1 X^{CR} \tag{8}$$

$$\dot{l}_a = k_2 X^{PZ} \tag{9}$$

Here, k_1 and k_2 are the kinetic coefficients. Such relationships are widely used in many empirical laws: for example, in Fourier's law for heat conduction (the heat flux is proportional to the gradient of temperature) and in Fick's law for diffusion (the flux of matter is proportional to the gradient of concentration).

(b) Parametric Study of the Model

The parameters employed in the model can be evaluated from experiments. Parameters such as γ_{tr}, σ_{tr}, and λ that are related to the material drawing can be determined in an independent test such as a test on neck formation. The kinetic coefficients, k_1 and k_2, and the parameters related to the material degradation, γ_0 and k, can be obtained from the first two steps of the CL growth.[10] Unfortunately, we do not have kinetic data of Ref. 1 except for lifetimes. However, it can be shown below that the rate constant k of the material degradation plays the major

role in the relation between creep and fatigue lifetimes in the case of discontinuous crack growth.

When the crack and the process zone are moving, the kinetic coefficients are responsible for a duration of the CL growth. Once the crack is arrested, γ_0 and k are responsible for the duration of the crack arrest. Figure 10 is a typical simulation of the model that mimics well the experimentally observed discontinuous crack growth. From the model we can also estimate lifetime based on the CL instability analysis.[10] For example, Figure 11 shows the effect of the rate constant k on lifetime for various stress levels. When the applied stress increases, the lifetime becomes less dependent on k. PE is known to show continuous crack growth under relatively high applied stress (e.g., $\sigma_\infty > 0.5\sigma_y$ in Ref. 11). In such a case, the kinetic coefficients play an important role in lifetime. In the case of the discontinuous crack growth shown in Figure 10, the duration of the crack propagation in total lifetime is quite small (around 15%). The duration of crack arrest plays a major part in the lifetime. Thus, the effect of the kinetic coefficients on the lifetime is very small and we assume that the ratio of the duration of crack propagation and crack arrest is constant for both creep and fatigue in Ref. 1.

Figure 12 shows the effect of the initial value of the fracture energy γ_0 on lifetime. When γ_0 increases, it requires a longer time period for the material in the process zone to be degraded to a value of J_1, leading to a longer lifetime for creep and fatigue. However, we found that the ratio of the rate constant of material degradation under fatigue, k_{fatigue}, and under creep, k_{creep}, for given lifetimes is practically independent on the value of γ_0 in Figure 12.

Thus, by choosing certain values of k_1, k_2, and γ_0 in such a way that the simulation shows the discontinuous CL growth, we can evaluate the rate constant under fatigue and creep from the known life-

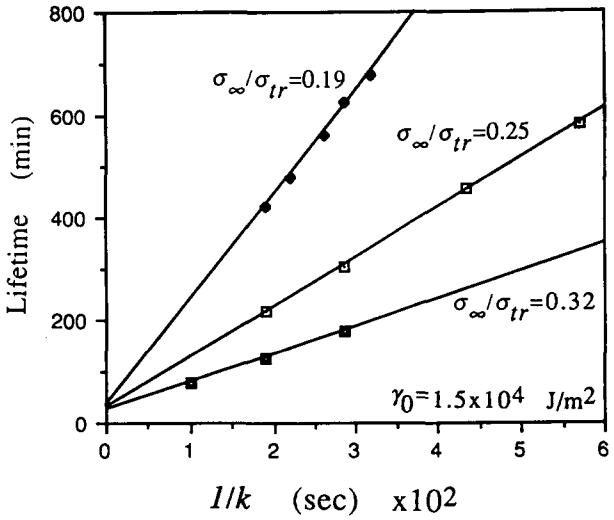

Figure 11 The calculated effect of the rate constant k on lifetime for various stress levels.

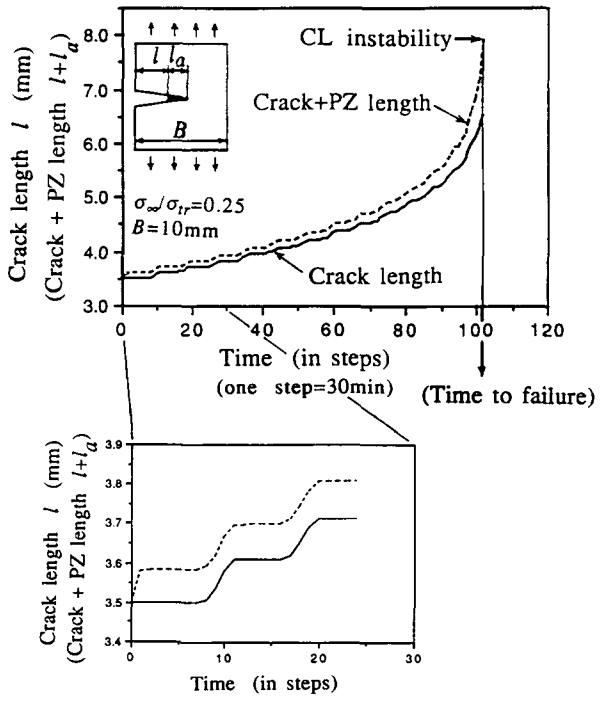

Figure 10 CL growth simulation.

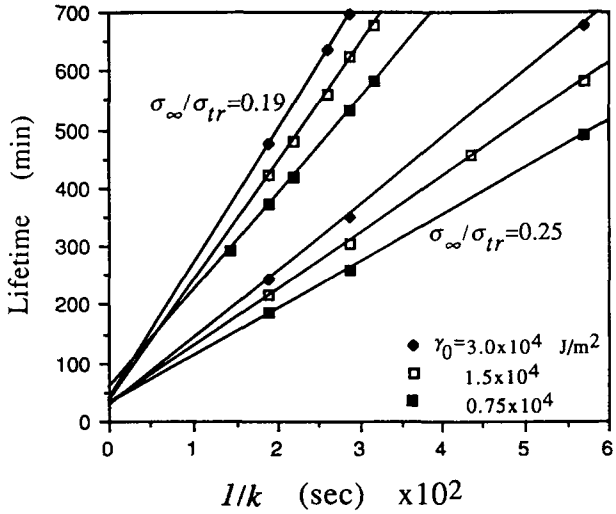

Figure 12 The calculated effect of the rate constant k on lifetime for various γ_0 and two applied stress levels.

Table I Material Properties and Fatigue/Creep Lifetime Data

Resin	M6006	M5502	M5202	M4903	TR140	TR418
Branch density* (butyl/1000 c)	0	0.8	1.2	2.0	2.3	4.6
Fatigue lifetime* t_f (min)	73	67	28	83	215	444
Creep lifetime* t_c (min)	65	138	245	2.46×10^3	2.35×10^4	2.75×10^6
Transformation stress σ_{tr} (MPa)	21.0	20.4	17.5	19.1	15.8	14.2
Young's modulus E_0 (GPa)	1.26	0.81	1.12	0.65	0.77	0.50
$\gamma_{tr}/(\lambda - 1)\sigma_{tr}$	1.05	1.05	1.05	1.05	1.05	1.05
$\ln(k_{creep}/k_{fatigue})$	0.728	−0.148	−1.521	−2.702	−3.993	−8.032
Onset temp of crystallization z_1 (°C)	122.5	120.8	119.7	117.9	117.2	115.3
Rate of crystallization z_2 (% intensity/°C)	0.21	0.20	0.16	0.21	0.19	0.16

Specimens and data * courtesy of Dr. N. Brown.

times. In this way, the difference in lifetime between creep and fatigue can be reduced to the difference in the rate constant, k, of the material degradation. The rate constant, k, depends on the type of loading but not on a particular applied stress, since the constant transformation stress σ_{tr} is acting along the process zone. The ratios of the rate constant of creep over that of fatigue that were obtained from the model using given lifetimes are listed in Table I.

MATERIAL CHARACTERIZATION

Lu and Brown suggested that the breaking of craze fibrils in the process zone due to disentanglement is a controlling factor of the creep crack growth in PE.[13] Indeed, Lu and Brown's suggestion is in agreement with the observation that the lifetime of PEs increases monotonically with an increase in branch density under creep loading conditions.[1] In addition to this, the cyclic loading has a mechanical fatigue effect, i.e., a bending of the fibrils. For example, it is well known that the tension–compression fatigue loading shortens the lifetime significantly in comparison with the tension–tension fatigue loading[17] since the compression loading compresses and crunches the buckled fibrils.[18] Thus, the rate constant of the material degradation under fatigue can be affected by the interplay of two factors. It is reported that the crystallization conditions change the morphological structure and therefore affect the fracture process.[19,20] Runt and Jaco also reported that the crystalline morphology has a significant influence on fatigue crack propagation.[21] Our purpose is to bridge the lifetime under fatigue and creep conditions with its crystalline behavior. Here, the crystallization kinetics of the materials tested in Ref. 1 are measured to characterize the material morphology.

(a) Nonisothermal Crystallization Kinetics Measurement

Each of the PE samples was compression-molded to a 5 mil-thick sample by using a hot press. The sample was cooled down to room temperature at 10°C/min in the press. A small piece of the molded sample was placed on a microscope glass slide and covered by a cover glass slide. The sample was then placed in a Mettler FP82 hot stage equipped with a Mettler FP80 temperature controller. The FP82 hot stage with the PE sample was placed on a Nikon Optiphot-Pol polarizing microscope equipped with adjustable polarizing filters. The lower filter was set at 180° and the entire optical system was moved as close to the hot stage as possible for optimum focus. The light source of the microscope was set at a constant setting. A 10× magnification object lens was used for this study. A Mettler photodiode was positioned in place of the camera projection lens of the microscope. The photodiode was coupled with the Mettler FP80 temperature controller to allow the measurement of temperature vs. light intensity detected by the photodiode. An IBM-PC was used for the data collection. Figure 13 is a schematic diagram of the instrumentation.

The polymer sample was heated to 180°C in the Mettler hot stage between the two microscope glass slides. The cover glass slide was pressed slightly to eliminate any trapped air bubbles in the molten sample. The sample was then cooled to 50°C at a rate of 10°C/min. The light intensity detected by

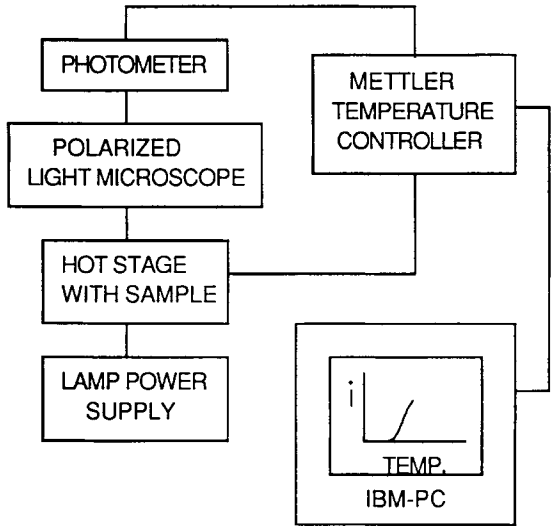

Figure 13 Schematic diagram of the equipment used for PE nonisothermal crystallization kinetics measurement.

the photodiode vs. temperature was collected by the IBM-PC. LOTUS123 and Graphwriter II software were used to reduce the digital data to graphic data.

(b) Results and Discussion

The depolarized optical microscope experiment described previously is very suitable for studying the quiescent crystallization of semicrystalline polymer such as PE. Figure 14 illustrates typical nonisothermal crystallization kinetics results of PE samples measured by this technique. A time period, referred to as the induction time, elapsed during which no depolarization of the light occurred for a given cooling rate; then, the photodiode began to detect the light passing through the sample as the molten polymer started to crystallize. As the crystallization process takes place under no external stress, the rate of light depolarization by the crystallizing sample is recorded as an increase in the light intensity. The percentage of the crystallized material from the melt can be calculated from the following equation:

$$\%X = [I_t - I_0]/[I_\infty - I_0] \qquad (10)$$

where $\%X$ is the % of the crystallized material from the melt; I_t, the intensity at any time during the cooling cycle; I_∞, the intensity when the entire crystallization is finished (maximum intensity); and I_0, the intensity before the crystallization begins (minimum intensity).

The primary and secondary crystallization processes described in Figure 14 are very dependent on the molecular structure of the polymer. Since linear PE copolymers (i.e., copolymer of ethylene with butene, hexene, octene, etc.) made by transition metal catalysis are heterogeneous mixtures, the degree of heterogeneity will affect these two processes significantly. The high density, low branch content material dominates the primary crystallization process to form a morphology "template." The quantity and the nature of the high-density material in the polymer mix, therefore, dictate the onset of the primary crystallization temperature, and, to some extent, the final morphology. Once the morphology "template" is formed, the high branch content "low-density" polymer starts to fill in "holes" in the preestablished spherulites and results in the final resin morphological structure as described in Figure 15.

CORRELATION OF CREEP AND FATIGUE

Our purpose is to correlate the rate constant of the material degradation under creep, k_{creep}, and under fatigue, k_{fatigue}, in terms of material morphology. Let us assume k_{creep} can be expressed by k_{fatigue} multiplied by a fatigue–creep correspondence factor, φ, depending only on the material morphology. Two parameters, z_1 and z_2, are used to describe the morphology. z_1 is the onset temperature of crystallization that reflects the primary crystallization process, and z_2, the rate of crystallization that reflects the secondary one. Thus, we assume

$$k_{\text{creep}}/k_{\text{fatigue}} = \varphi(z_1, z_2) \qquad (11)$$

Taking the logarithm of eq. (11),

$$\ln(k_{\text{creep}}/k_{\text{fatigue}}) = \ln \varphi(z_1, z_2) \qquad (12)$$

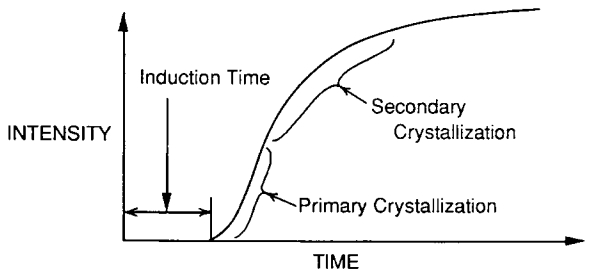

Figure 14 Crystallization processes.

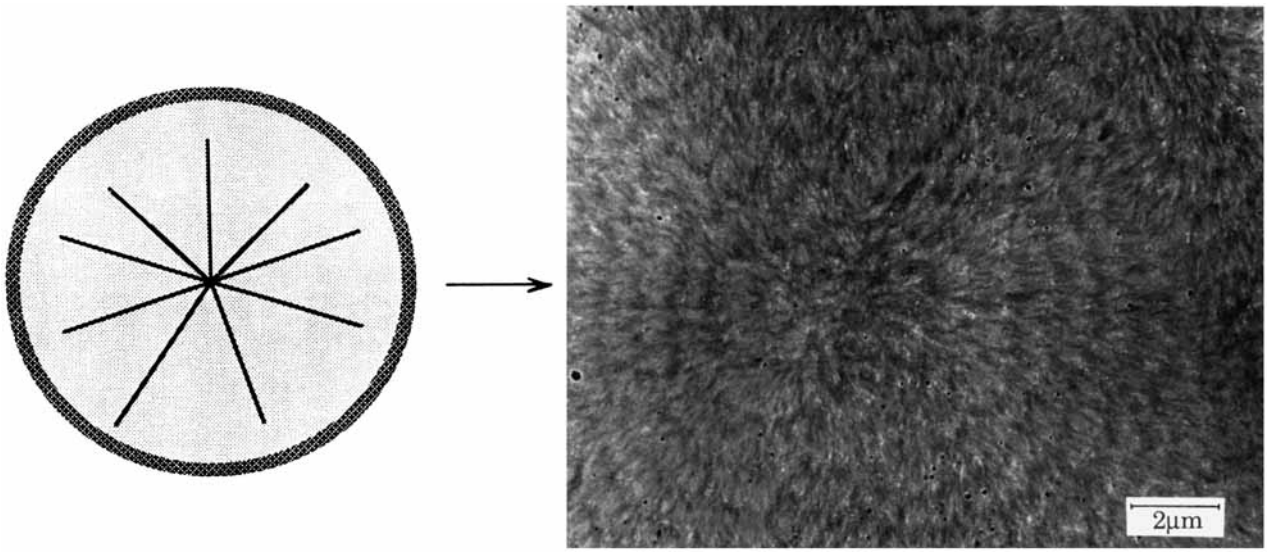

Figure 15 Development of spherulitic morphology in linear low-density PE (LLDPE): (1) structure dominated by low branch content "high-density" material to form morphology "template"; (2) high-branch content "low-density" material fills in "holes and wedges" in preestablished spherulites to form final resin spherulitic structure.

The function $\ln \varphi(z_1, z_2)$ is approximated by quadratic form of two variables, z_1 and z_2, as follows:

$$\ln \varphi(z_1, z_2) = a_0 + \sum_{i,j=1}^{2} a_{ij}(z_i - c_i)(z_j - c_j)$$

where the coefficients a_0, a_{ij}, and c_i, c_j are determined from the data of crystallization kinetics and rate constants of degradation and are summarized in Tables I and II. Thus, the fatigue–creep correspondence factor φ is approximated by the two-dimensional normal distribution density of z_1 and z_2.

Figure 16 illustrates the fatigue–creep correspondence factor as a function of the morphological characteristics z_1 and z_2. Hollow dots represent the experimental data for five different materials, and solid dots, the projection of the data into one plane (z_2 = constant). As a function of just one variable z_1, the correlation between the rate constants under fatigue and under creep is nonmonotonic. Especially, M5202 resin (branch density = 1.2) shows remarkably low fatigue lifetime (= high negative value in $\ln \varphi$). However, the secondary crystallization, i.e., the parameter z_2, can differentiate this material from others. This suggests that the secondary crystallization has a negative effect on fatigue lifetime. By introducing two parameters z_1 and z_2 to reflect the material morphology, one can express the fatigue–creep correspondence factor as a smooth function. This demonstrates the correlation between the fracture phenomena and the molecular architecture and the possibility to bridge the two.

Once the fatigue–creep correspondence factor φ is determined, measuring morphological characteristics allows us to estimate a long-term creep lifetime from a short-term fatigue test using the model of the CL growth. To further examine this phenomenological analysis, additional experiments using materials with controlled morphology are required.

Table II Parameters of the Fatigue-Creep Correspondence

α_0	α_{11}	$\alpha_{12} = \alpha_{21}$	α_{22}	z_1	z_2
−12.34	−8.203	−2.914	−94.05	82.4	1.40

CONCLUSIONS

1. The rate constant of the degradation process of the material within the process zone can be considered as a controlling factor in a slow crack growth of PE under relatively low applied stress.
2. The preliminary study demonstrates the possibility to bridge the fracture phenomena with the molecular architecture.
3. The model employed here is perhaps suitable

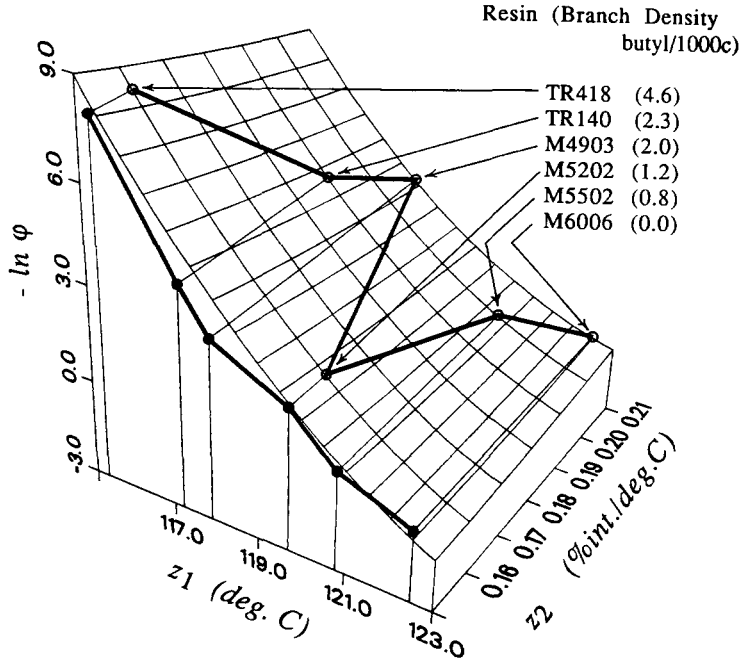

Figure 16 Fatigue-creep correspondence factor φ.

as a tool to establish an accelerated test for long-term service life.

The authors especially wish to thank Professor N. Brown at the University of Pennsylvania for providing us with the specimens and data of Ref. 1. Financial support from the Gas Research Institute (Contract No. GRI 5088 260 1684) and the Air Force Office of Scientific Research (Contract No. FED AFOSR-89-0105) is greatly appreciated. We would like to thank Drs. C. P. Bosnyak and K. Sehanobish from the Dow Chemical Co. for useful discussions and suggestions. The authors also wish to acknowledge the Electron Microscope Facility of the Research Resources Center, University of Illinois at Chicago, which provided the equipment and assistance in conducting this study.

REFERENCES

1. Y. Zhou, Y. Huang, X. Lu, and N. Brown, in *Plastic Fuel Gas Pipe Symposium Proceedings,* San Francisco, CA, Oct. 3–5, 1989.
2. Y. Zhou, Y. Ling, X. Lu, and N. Brown, in *Proceedings of the International Gas Research Conference,* Tokyo, Japan, Nov. 6–9, 1989.
3. H. Nishimura, T. Shishido, M. Nakakura, and H. Shibano, in *Proceedings of the Ninth Plastic Fuel Gas Pipe Symposium,* New Orleans, 1985, p. 70.
3. K. Chaoui, J. J. Strebel, A. Chudnovsky, and A. Moet, in *Proceedings of the International Gas Research Conference,* Tokyo, Japan, Nov. 6–9, 1989.
5. J. J. Strebel and A. Moet, *J. Mater. Sci.,* **26,** 5671 (1991).
6. M. L. Kasakevich, A. Moet, and A. Chudnovsky, *Polymer,* **31,** 435 (1990).
7. H. Nishimura and I. Narisawa, *Polym. Eng. Sci.,* **31,** 399 (1991).
8. R. T. Reynolds and C. C. Lawrence, *J. Mater. Sci.,* **26,** 6107 (1991).
9. M. B. Barker, J. Bowman, and M. Bevis, *J. Mater. Sci.,* **18,** 1095 (1983).
10. K. Kadota and A. Chudnovsky, *Polym. Eng. Sci.,* to appear.
11. X. Lu, R. Qian, and N. Brown, *J. Mater. Sci.,* **26,** 917 (1991).
12. K. Kadota, A. Chudnovsky, J. J. Strebel, and A. Moet, in *Proceedings of the ANTEC'91,* Montreal, Canada, 1991, p. 2180.
13. X. Lu and N. Brown, *J. Mater. Sci.,* **26,** 612 (1991).
14. A. Stojimirovic and A. Chudnovsky, *Int. J. Fracture,* to appear.
15. K. Kadota and A. Chudnovsky, in *Proceedings of the ASME Winter Annual Meeting,* Atlanta, GA, Dec. 1–6, 1991, Vol. MD-29, p. 101.
16. S. N. Zhurkov, *Int. J. Fracture Mech.,* **1,** 311 (1965).
17. A. Moet, *GRI Annual Meeting,* Gas Research Institute, 8600 West Bryn Mawr Ave., Chicago, IL 60631, Sept. 5, 1991.
18. Y. Zhou and N. Brown, *J. Mater. Sci.,* to appear.
19. U. W. Gedde and J. F. Jansson, *Polymer,* **26,** 1469 (1985).
20. X. Lu and N. Brown, *Polymer,* **28,** 1505 (1989).
21. J. Runt and M. Jaco, *J. Mater. Sci.,* **24,** 1421 (1989).

Received June 11, 1992
Accepted November 17, 1992